Title

Adaptive Multirate Mass Transfer (aMMT) Model: A New Approach to Upscale Regional-Scale Transport Under Transient Flow Conditions

Journal

Water Resources Research, 56(2)

ISSN

0043-1397

Authors

Guo, Zhilin
Henri, Christopher V
Fogg, Graham E
et al.

Publication Date

2020-02-01

DOI

10.1029/2019wr026000

Peer reviewed

Water Resources Research

RESEARCH ARTICLE
10.1029/2019WR026000

Adaptive Multirate Mass Transfer (aMMT) Model: A New Approach to Upscale Regional-Scale Transport Under Transient Flow Conditions

Zhilin Guo[1,2], Christopher V. Henri[2], Graham E. Fogg[2], Yong Zhang[3], and Chunmiao Zheng[1]

[1]Guangdong Provincial Key Laboratory of Soil and Groundwater Pollution Control, School of Environmental Science and Engineering, Southern University of Science and Technology, Shenzhen, China, [2]Hydrologic Sciences, University of California, Davis, CA, USA, [3]Department of Geological Sciences, University of Alabama, Tuscaloosa, AL, USA

Key Points:
- Adaptive Multirate Mass Transfer (aMMT) model was developed to upscale transport under transient flow conditions
- aMMT reproduces tracer breakthrough tails observed in heterogeneous media under transient flow, diffusion-dominant transport conditions
- aMMT fails if the primary flow direction changes in time and the coefficients are fitted by previous flow conditions

Supporting Information:
- Supporting Information S1

Correspondence to:
Z. Guo,
guozl@sustech.edu.cn

Citation:
Guo, Z., Henri, C. V., Fogg, G. E., Zhang, Y., & Zheng, C. (2020). Adaptive Multirate Mass Transfer (aMMT) model: A new approach to upscale regional-scale transport under transient flow conditions. *Water Resources Research*, *56*, e2019WR026000. https://doi.org/10.1029/2019WR026000

Received 23 JUL 2019
Accepted 27 JAN 2020
Accepted article online 30 JAN 2020

Abstract The long-term evaluation of regional-scale groundwater quality needs efficient upscaling methods for transient flow. Upscaling techniques, such as the Multirate Mass Transfer (MRMT) method with constant upscaling parameters, have been used for transport with steady-state flow, yet the upscaling parameters (i.e., rate coefficients) may be time dependent. This study proposed and validated an adaptive MRMT (aMMT) method by allowing the mass transfer coefficients in MRMT to change with the flow field. Advective-dispersive contaminant transport simulated in a 3-D heterogeneous medium was used as a reference solution. Equivalent transport under homogeneous flow conditions was evaluated by applying the MRMT and aMMT models for upscaling. The relationship between mass transfer coefficients and flow rates was fitted under steady-state flow driven by various hydraulic gradients. A power law relationship was obtained, which was then used to update the mass transfer coefficients in each stress period under transient flow conditions in the aMMT method. Results indicated that for advection-dominated transport, both the MRMT and aMMT methods can upscale the anomalous transport dynamics affected by subgrid heterogeneity under transient flow conditions. Whereas for diffusion-dominated systems, the MRMT model failed to capture the tails of tracer breakthrough curves after the boundary condition changed, but the results from the aMMT model were significantly improved. However, if the overall flow direction changed, both MRMT and aMMT failed to represent the breakthrough curve tail generated by the heterogeneous system. The results point toward a promising path for upscaling transport in complex aquifers with transient flow.

1. Introduction

Deterioration of groundwater quality has become a major global issue (e.g., Anastasiadis, 2004; Chae et al., 2004; Nativ, 2004; Nolan et al., 2002; Sinha & Elango, 2019; Sivasankar et al., 2013; Vengosh et al., 2002; Zektser & Everett, 2004; Zhang et al., 2006) and will likely continue as such during the coming decades or centuries depending on the aquifer renewal rate and groundwater age distributions (e.g., Edirisinghe et al., 2016; Fogg & LaBolle, 2006; Fogg et al., 1999; Li et al., 2015; Tompson et al., 1999; Weissmann et al., 2002). Regional-scale groundwater quality management models that adequately represent regional transport phenomena are needed to support the long-term evaluation of groundwater quality and identify decadal time scale management strategies needed to reverse the ongoing degradation (Fogg & LaBolle, 2006; Fogg & Zhang, 2016; Guo, Fogg, & Henri, 2019).

Impacts of aquifer heterogeneity on solute transport have been reported in many studies, including the early arrival of contaminants caused by the preferential flow in well-connected channels and the long-time tailing behavior resulting from transport through low-permeability materials in alluvial settings (e.g., Bianchi et al., 2011; Brusseau & Guo, 2014; Brusseau et al., 2007, 2011; Dearden et al., 2013; Fogg & LaBolle, 2006; Fogg & Zhang, 2016; Fogg et al., 2000; Guo & Brusseau, 2017; LaBolle & Fogg, 2001; Matthieu et al., 2014; Seyedabbasi et al., 2012; Zheng & Gorelick, 2003). Findings of these studies indicate the importance of representing medium heterogeneity for regional groundwater quality management. However, the fine-resolution hydraulic properties cannot be mapped explicitly in most regional models, resulting in a coarse resolution of velocity that challenges the applicability of the classical advection-dispersion equation (ADE) in reproducing the real-world complex transport behavior (Zheng et al., 2010).

Accordingly, regional transport models capable of using regional velocity fields from coarse-resolution flow models while also representing the appropriate transport phenomena are needed (Fogg & LaBolle, 2006; Fogg & Zhang, 2016).

In addition, the transient boundary conditions and velocity fields caused by past and possible future changes of land and/or water uses should also be captured by the regional water quality management models. The groundwater quality will be impacted by the changing contaminant sources and velocity fields caused by changes in recharge, groundwater and surface water interaction, and/or changing pumping rates and well distributions. Therefore, the upscaled regional model needs to not only characterize the effect of medium heterogeneity on transport but also be sufficiently general to represent transport under transient flow driven by temporally variable boundary conditions.

Non-Fickian transport, characterized by early arrivals and/or late-time tails in solute breakthrough curves (BTCs), has been frequently observed (Baeumer et al., 2015; Benson et al., 2001; Bolster et al., 2010; Dentz et al., 2004; Sokolov & Klafter, 2006; Zhang et al., 2009). To overcome the inability to represent non-Fickian or nonergodic behaviors, nonlocal transport methods have been developed in the past decades. Among them, we can cite the continuous time random walk (CTRW) framework (Berkowitz et al., 2006; Berkowitz & Scher, 1995, 1998), fractional ADEs (fADEs) (Benson et al., 2000a, 2000b), multirate mass transfer (MRMT) model (Haggerty & Gorelick, 1995; Harvey & Gorelick, 2000; Silva et al., 2009), and other mass exchange models such as matrix diffusion with memory functions (Carrera et al., 1998; Carrera & Neuman, 1986). These time-nonlocal transport methods have been demonstrated to successfully describe solute transport in conditions where the boundary conditions are steady (e.g., Benson et al., 2001; Berkowitz et al., 2006; Cortis & Berkowitz, 2005; Feehley et al., 2000; Harvey & Gorelick, 2000; Pedretti et al., 2014; Willmann et al., 2008; Zhang, Benson, Meerschaert, & LaBolle, 2007; Zinn & Harvey, 2003). However, these methods may fail under more complex and realistic conditions such as transient flow. For example, Guo, Fogg, and Henri (2019) tested the applicability of MRMT under different transient conditions, using flow systems changing at the local or regional scale. Potential factors that impact the performance of upscaling methods, including temporal variations in mass transfer rate coefficients and mass distributions, were investigated. Results indicated that MRMT with a constant mass transfer rate coefficient failed to describe the transient transport processes in heterogeneous aquifers because the mass transfer rates changed with the transient flow field. The failure of the MRMT model in upscaling transport under the transient condition may also provide insights on possible limitations of the other upscaling methods under transient conditions, since most of the time-nonlocal transport models mentioned above were found to be mathematically equivalent or similar (Berkowitz et al., 2006; Dentz & Berkowitz, 2003; Lu et al., 2018).

Guswa and Freyberg (2000) studied the relative importance of slow advection and diffusion for transport within low permeability zones for systems with different structures. Results indicated the significant impacts of regional flow field on the elution of contaminants if slow advection is dominant in the system. Contrarily, if diffusion dominates the transport dynamics, solute transport will not be impacted by changes in the regional flow. Gorelick et al. (2005) generated three-dimensional (3-D) conductive dendritic structures embedded in realizations of low permeability, homogeneous matrix and presented a relationship between the mass transfer coefficient and the conduit/matrix conductivity ratio that relates to the flow field. Nagy (2009) demonstrated the effects of the convective velocity on the mass transfer coefficients by investigating the mass transport through a biocatalytic membrane layer. Nissan et al. (2017) showed the effects of a time-varying velocity field on solute transport by both experiments and modeling in 1-D and 2-D scale. These studies highlighted the relation between velocity and mass transfer rate coefficients and further demonstrated that this correlation could be the main reason causing the failure of the MRMT method with constant upscaling parameters in upscaling transport under the transient flow condition. However, the detailed relationship has, to the best knowledge of the authors, not been reported yet.

In this study, an adaptive MRMT (aMMT) method is described based on an assumed relationship between mass transfer rate coefficients and velocities. The assumption is then tested by upscaling groundwater flow and solute transport simulated within a fully heterogeneous domain. The aMMT method is presented by incorporating the impact of temporal variation of velocity into the MRMT process. The capability of the aMMT method to describe dynamics of solute transport under transient flow, especially the late-time tails in BTCs with changed boundary conditions, will be systematically investigated for the first time.

Performances of the two upscaling methods, aMMT and MRMT, in representing transport under transient flow will be evaluated under different flow conditions. This work provides insights on anomalous transport in realistically heterogeneous systems and helps illuminate a path toward development of groundwater quality management models.

2. The aMMT Method

2.1. Model Development

Guo, Fogg, and Henri (2019) found that the conventional MRMT model with constant mass transfer rate coefficients cannot upscale transport under transient flow conditions, which is due to the mass transfer rate coefficients changing with the transient flow fields. We therefore hypothesize that making the mass transfer rate coefficients functions of velocity might better represent anomalous transport under transient flow conditions. In this study, we started from the flow and transport models and then modified the MRMT method as an upscaling technique that can adapt to transient flow conditions.

2.1.1. Classical Advection-Dispersion Model

The 3-D groundwater flow is described by the following flow equation (McDonald & Harbaugh, 1988):

$$\frac{\partial}{\partial x}\left(K_{xx}\frac{\partial h}{\partial x}\right)+\frac{\partial}{\partial y}\left(K_{yy}\frac{\partial h}{\partial y}\right)+\frac{\partial}{\partial z}\left(K_{zz}\frac{\partial h}{\partial z}\right)+W=S_s\frac{\partial h}{\partial t}, \tag{1}$$

where K_{xx}, K_{yy}, and K_{zz} (LT^{-1}) denote hydraulic conductivity along the x, y, and z coordinate axes; h (L) is the potentiometric head; W (T^{-1}) is a volumetric flux per unit volume representing sources ($W>0$) and/or sinks ($W<0$) of water; S_S (L^{-1}) is the specific storage of the porous material; and t (T) is time.

The 3-D solute transport is described by the classical ADE (Zheng & Wang, 1999):

$$\frac{\partial(\theta c)}{\partial t}=\frac{\partial}{\partial x_i}\left(\theta D_{ij}\frac{\partial c}{\partial x_j}\right)-\frac{\partial}{\partial x_i}(\theta v_i c)+q_s c_s+\sum r_n, \tag{2}$$

where θ (dimensionless) is the porosity of the subsurface medium; c (ML^{-3}) is the concentration of the dissolved solute; x_{ij} (L) is the distance along the respective Cartesian coordinate axis; D ($\mathrm{L}^2\,\mathrm{T}^{-1}$) is the hydrodynamic dispersion coefficient tensor; v_j (LT^{-1}) is the seepage or linear pore water velocity vector; q_s (T^{-1}) is the volumetric flow rate per unit volume of aquifer representing fluid sources (positive) or sinks (negative); c_s is the concentration of the source or sink flux; and $\sum r_n$ ($\mathrm{ML}^{-3}\,\mathrm{T}^{-1}$) denotes mass exchange due to chemical reactions.

2.1.2. MRMT Model

The MRMT model, which fails to represent the transient transport as shown in Guo, Fogg, and Henri (2019), has been described by Haggerty and Gorelick (1995) as

$$\frac{\partial c_m}{\partial t}+\sum_{j=1}^{N_{im}}\beta_j\frac{\partial c_{im,j}}{\partial t}=\zeta(\mathrm{c}_m) \tag{3}$$

$$\frac{\partial c_{im,j}}{\partial t}=\frac{\alpha_j}{R_{im,j}}\left(\mathrm{c}_m-c_{im,j}\right) \tag{4}$$

where c_m is the chemical concentration in the mobile zone; c_{im} is the concentration in the jth immobile zone; N_{im} (dimensionless) is the total number of the distinct immobile zones; α_j (T^{-1}) is the first-order mass transfer rate coefficient between the mobile zone and the jth immobile zone; β_j (dimensionless) is the capacity coefficient representing the ratio of mass in the jth immobile zone and the mobile zone when solute transport reaches equilibrium; and $\zeta(\mathrm{c}_m)$ is the advection-dispersion operator defining the displacement of mobile solutes:

$$\zeta(\mathrm{c}_m)=\nabla\cdot\left(\frac{\mathbf{D}\nabla c_m}{R_m}\right)-\nabla\cdot\left(\frac{\mathbf{q}c_m}{\theta_m R_m}\right) \tag{5}$$

Table 1
Parameters Defined for a Finite Spherical Diffusion Model

	For $j = 1, \dots, N_{im} - 1$	For $j = N_{im}$ (final term)
α_j	$j^2\pi^2\alpha$	$\frac{15\alpha\left[1-\sum_{j=1}^{N_{im}}\frac{6}{j^2\pi^2}\right]}{1-\sum_{j=1}^{N_{im}}\frac{90}{j^4\pi^4}}$
β_j	$\frac{6}{j^2\pi^2}\beta$	$\left[1-\sum_{j=1}^{N_{im}}\frac{6}{j^2\pi^2}\right]\beta$

In the random heterogeneous combination of hydrofacies built in this study (section 2.2.1), diffusion is the major mechanism for solute particles to move into and out of the relatively low permeability hydrofacies (i.e., clay). Hence, the probability for solute particles to change phases (mobile vs. immobile) depends on the residence time for particles in the low permeability hydrofacies. This is analogous to the MRMT between the mobile phase and the multiple, spherical, immobile domains (Haggerty et al., 2000; Haggerty & Gorelick, 1995). Hence, we apply the spherical diffusion model to approximate anomalous transport in the hydrofacies model. A similar approximation was used by Zhang, Benson, and Baeumer (2007). Indeed, the BTCs resulting from the heterogeneous simulation (described in section 2.2) can be effectively fitted using the spherical diffusion model, which simulates the transfer of solute mass into and out of theoretical immobile spheres (Haggerty & Gorelick, 1995). Haggerty and Gorelick (1995) revealed the equivalency between the MRMT model and the diffusion models by defining a series of N_{im} first-order rate coefficients (α_j, $j = 1, \dots, N_{im}$) and N_{im} capacity coefficients (β_j), which are defined for the spherical diffusion model in Table 1.

Using the spherical diffusion model, two parameters have to be fitted: the diffusion rate coefficient α (T^{-1}) defined as $\alpha = \frac{D_{am}}{a^2}$, where D_{am} (L^2/T) is the apparent diffusion coefficient and a (L) is the radius of the spherical blocks; and the total capacity coefficient β (dimensionless) representing the ratio of the total contaminant mass in the immobile zones and the total mass in the mobile zone at equilibrium. β can be calculated by summing the capacity ratio of each immobile domain:

$\beta = \sum_{j=1}^{N_{im}} \beta_j = \sum_{j=1}^{N_{im}} \frac{R_{im,j}\theta_{im,j}}{R_m\theta_m}$, where θ_m (dimensionless) is the porosity of the mobile zone; $\theta_{im,j}$ (dimensionless) is the porosity of the jth immobile zone ($j = 1, \dots, N_{im}$); R_m (dimensionless) is the retardation factor in the mobile domain; and $R_{im,j}$ (dimensionless) is the retardation factor in the jth immobile zone (j = 1, … , N_{im}). The MRMT model is theoretically equivalent to the diffusion models when an infinite series of rate/capacity coefficients is used (Haggerty & Gorelick, 1995). However, Salamon et al. (2006) showed that the multirate coefficient series can be truncated (the final terms of the truncated multirate series are listed in Table 1) and the solution converges for a relatively small number of terms (i.e., 6 to 8). In this study, 10 terms (of rate α_j and capacity coefficients β_j) were considered. The values of each α_j and β_j are estimated using the series described in Table 1, and they are related to a single pair of parameters: the apparent diffusion coefficient α and the total capacity coefficient β. Only these two parameters have, therefore, to be calibrated in the following.

2.1.3. aMMT Model

We incorporate the velocity into equations (3) and (4) to capture the changing flow fields for the aMMT method using

$$\alpha(t) = f_1(v(t)) \tag{6}$$

$$\beta(t) = f_2(v(t)) \tag{7}$$

where f_1 and f_2 are the function operators that can be determined by the relationship between the calibrated α and v and β and v, respectively; and the pore velocity v (LT^{-1}) is calculated for each scenario with a specified hydraulic gradient ∇h across the entire flow domain under steady state by

$$v = \frac{K_{eq}\nabla h}{\theta_m} \tag{8}$$

where K_{eq} is the hydraulic conductivity of the equivalent homogeneous medium derived from the regional-scale heterogeneous medium and θ_m is the porosity for the mobile zone. The assumed relationship (7)–(9) is tested by upscaling the flow and transport processes simulated in the heterogeneous field using MRMT in the next section. It is noteworthy that the method (7)–(9) in its present form is adapted to a diffusion

Table 2
Hydraulic Conductivity, K, and Porosity of the Four Hydrofacies for the Heterogeneous Simulations

Hydrofacies	K (m/day)	Porosity	Direction and mean length		
			Strike (m)	Dip (m)	Vertical (m)
Gravel	124	0.25	360	500	9.6
Sand	45	0.25	200	265	8.6
Silt	3	0.25	380	350	13.8
Clay	0.00013	0.37	880	700	16.9

model, where the apparent diffusion coefficient α and the total capacity coefficient β determine each pair of the mass transfer rate coefficient (α_j) and capacity coefficient (β_j) (Table 1). Each α_j or β_j is then a function of the temporally variable velocity, through the multirate series defined in Table 1. If another classical MRMT model (different from the diffusion model; as listed in Table 1 in Haggerty et al., 2000) is used, the velocity dependence for each α_j and β_j needs to be recalibrated.

2.2. Reference Model With Explicit Representation of Heterogeneity

2.2.1. Geostatistical Simulation of Heterogeneity

The computer program T-PROGS, which is based on a transition probability-Markov chain random-field approach described by Carle and Fogg (1996, 1997), Carle (1997), and Carle et al. (1998), was used to generate 3-D heterogeneous domains. The hydrofacies categories are identified by interpretation of well logs collected from field sites. Transition probabilities are measured and used to conditionally simulate realizations of hydrostratigraphy for each depositional (strike, dip, and vertical) direction and to generate 3-D realizations of random fields of hydrofacies. In this study, 245 geological boreholes collected from the Tucson International Airport Area (TIAA) Superfund site (Zhang & Brusseau, 1998) were interpreted and categorized into four hydrofacies, which are clay (with the volumetric proportion of 42.4%), silty sand (17.7%), sand (19.6%), and gravel (20.3%). Vertical lengths for each hydrofacies were determined directly from the borehole logs, and strike and dip lengths were estimated through both analysis of the data and geologic interpretation (Carle & Fogg, 1997; Carle et al., 1998). Mean lengths of the four hydrofacies in the dip, strike, and vertical directions are summarized in Table 2. Based on the resulting Markov chain model of transition probability, the geostatistical conditional realizations were generated on a grid of 250 (strike) × 250 (dip) × 70 (vertical) nodes with 20.0 m × 20.0 m × 1.0 m spacing (Figure 1a). The top of the generated domain coincides with the water table. More details on the domain generation were discussed in Guo, Fogg, Brusseau, et al. (2019).

Guo, Fogg, and Henri (2019) presented results for 10 realizations, where the high-K facies percolate or interconnect in all three dimensions. Accordingly, Guo, Fogg, and Henri (2019) found that the 10 realizations of the hydrofacies model produced very similar patterns of anomalous transport, including preferential flow and late-time BTC tails. In this study, as the purpose is to demonstrate the methodology development of aMMT and test the performance of aMMT and MRMT, we needed only one realization of the hydrofacies to fulfill the purpose of the study. Furthermore, the need for multiple realizations is reduced by the fact that the solute source is a nonpoint source and hence ergodicity of the source term with respect to system heterogeneity is not a concern.

2.2.2. Groundwater Flow and Solute Transport Models

Groundwater flow was simulated using MODFLOW, a 3-D finite-difference groundwater flow solver (McDonald & Harbaugh, 1988; Harbaugh et al., 2000), and using the same grid as the geostatistical model. General head boundaries were used along the two borders that are perpendicular to the flow direction, to form a natural gradient to induce groundwater flow. The other four borders were no-flow boundaries. Spatially variable hydraulic conductivities (K) and porosities were assigned to individual cells according to the categories of hydrofacies for the corresponding cells from the geostatistical realization (Table 2). K and porosity for each hydrofacies used in the model were determined according to information generated from geologic borehole-logs, pumping tests, and historic data collected for the TIAA Superfund site (Zhang & Brusseau, 1999).

Solute transport was modeled using the code RW3D that solves advection, dispersion, and MRMT using the random walk particle tracking approach (Fernàndez-Garcia et al., 2005; Henri & Fernàndez-Garcia, 2014; Henri & Fernàndez-Garcia, 2015; Salamon et al., 2006). Longitudinal, transverse, and vertical dispersivities representing grid-scale dispersion were set to 1.0, 0.1, and 0.01 m, respectively. Hydrofacies models with the built-in heterogeneity structure can capture most of the dispersion in solute transport, and hence, a relatively small dispersivity can be used to capture the subgrid heterogeneity (see also the discussion in Weissmann et al., 2002, for the selection of small dispersivities for fine-resolution hydrofacies models). The aqueous diffusion coefficient was 7.6×10^{-5} m^2/day, determined using the Trichloroethylene (TCE) data measured at the TIAA Area Superfund site (Zhang & Brusseau, 1999).

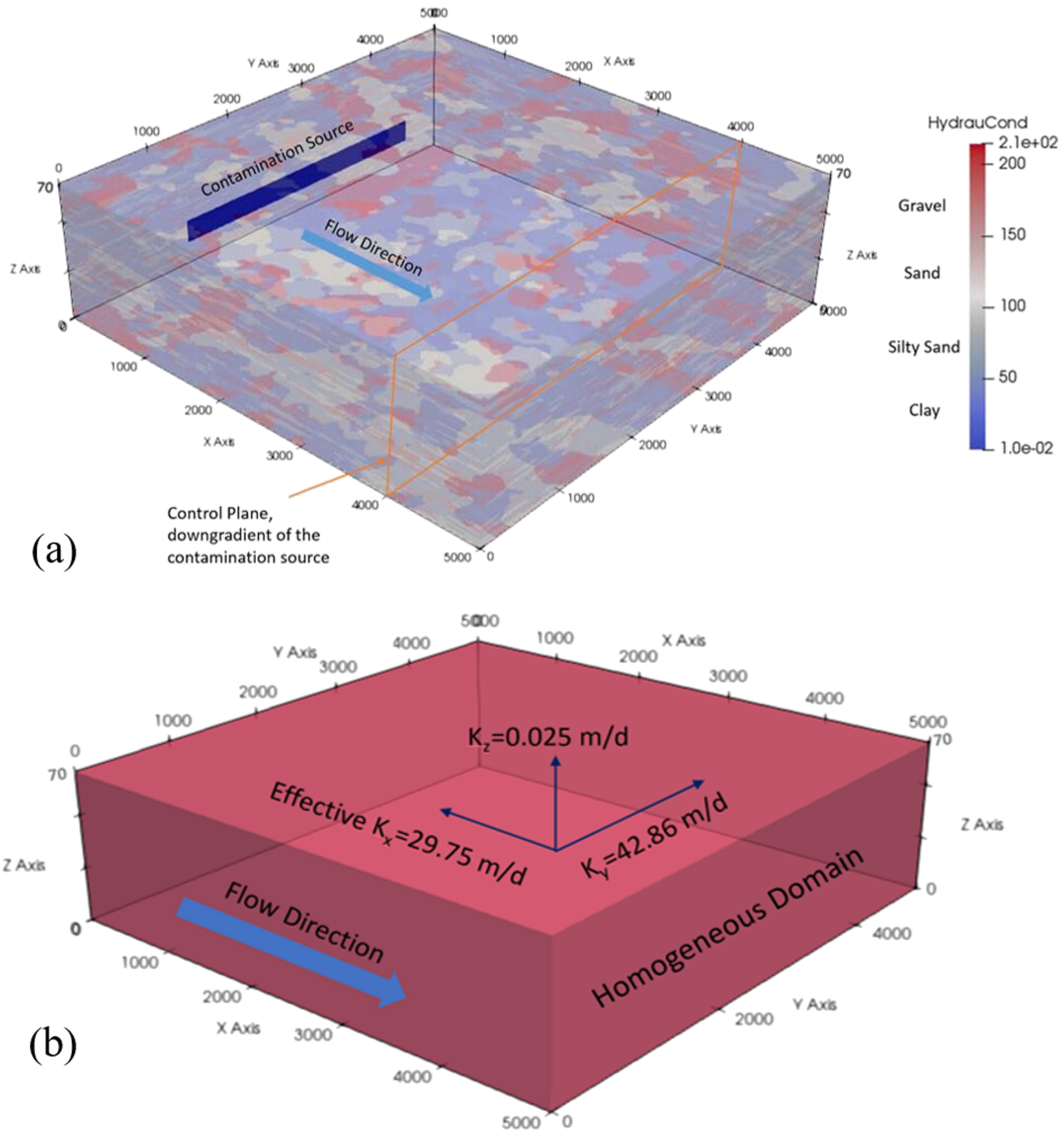

Figure 1. Three-dimensional view of realization #1 for the hydrofacies model and the conceptual model set up for solute transport (a). Effective K values in x, y, and z directions are shown for the homogeneous equivalent system (b).

2.3. Upscaled Model

2.3.1. Effective Flow Field

The equivalent flow fields for homogeneous simulations (Figure 1b) were generated by upscaling the heterogeneous K fields, similar to the procedure of Liu et al. (2004). Specified head boundaries were applied for the two sides along the x axis of the domain, and no-flow boundaries were defined for the other four boundaries. As for the heterogeneous case, a general hydraulic gradient of 0.001 was imposed across the domain. The equivalent K along the x direction was computed based on the steady-state flow rate through the domain for heterogeneous simulations using Darcy's law. The equivalent K values in y and z directions were determined the same way, using the rates of flow across the side and bottom edges of the heterogeneous domain, respectively. The relative difference in flow between the homogeneous and heterogeneous cases was below 0.5%, indicating that the homogenous equivalent parameter preserves the average velocity and water balance observed in the heterogeneous case. For the transient flow that we simulated, the difference for the water budget was also less than 1%, indicating preservation of flow fields under the transient conditions.

Table 3
The Bestfit α, the Calculated β (for MRMT and aMMT), and the Calculated D_a Used for Simulations With Different Velocities

Hydraulic gradient (m/m)	v (m/day)	β (−)	α (day^{-1})	D_a (−)
(a) Horizontal flow only				
0.01	1.488	2	4.0E−06	0.028
0.008	1.322	2	3.8E−06	0.030
0.005	0.875	2	3.3E−06	0.040
0.003	0.595	2	2.6E−06	0.046
0.001	0.229	2	2.0E−06	0.092
0.0005	0.124	2	1.2E−06	0.104
0.0003	0.081	2	1.0E−06	0.133
0.0001	0.030	2	8.0E−07	0.292
(b) Vertical flow only				
0.2	0.0333	2	1.2E−05	0.049
0.15	0.0288	2	1.1E−05	0.051
0.1	0.0179	2	8.0E−06	0.060
0.08	0.0154	2	4.0E−06	0.035
0.05	0.0096	2	3.0E−06	0.042
0.03	0.0063	2	2.0E−06	0.043
0.01	0.0021	2	1.0E−06	0.065
0.005	0.0011	2	4.0E−07	0.048
0.003	0.0007	2	3.0E−07	0.059

2.3.2. Upscaling Transport Using MRMT Method

The mass transfer rate coefficients used in the MRMT equation (4) were determined by fitting the BTCs for the homogeneous simulation to the corresponding BTCs for the heterogeneous simulation at the vertical control planes crossing the domain located at $x = 4{,}000$ m. The fitted coefficients were applied to the entire domain as we assumed that the mass transfer rates are not significantly related to the advection time based on results from previous studies (Guo, Fogg, & Henri, 2019; Haggerty et al., 2004). Diffusion coefficient was the same as the one used for the heterogeneous simulations. Dispersivity was calibrated by fitting the spreading of BTCs for the homogeneous simulation to the BTCs for the heterogeneous simulation. Porosity for the mobile zone (θ_m) was determined by matching the arrival time of solutes captured by the BTC and the center of the plume for the heterogeneous simulations. The BTCs plotted using the relative mass flux versus time were used to evaluate the performance of the MRMT and aMMT models. An adaptive kernel density estimator method (Pedretti & Fernandez-Garcia, 2013) was used to reconstruct the BTCs to mitigate subsampling effects.

2.3.3. Relationship Between Mass Transfer Parameters and Velocity

Simulations were conducted with either the horizontal or vertical flow under steady-state flow conditions for heterogeneous and upscaled homogeneous domains to determine the relationship between mass transfer rate coefficients and velocities. The scenarios were simulated with flow in either direction to illustrate the existence of the relationship regardless structure of the domain, as the stratification and the connectivity among high K zones are different in two directions.

For the simulations with the steady-state horizontal flow only, 100,000 solute particles were released initially from a vertical plane of 3,000 m wide and 10 m long perpendicular to the flow direction located at $x = 500$ m. Preliminary tests showed that a total number of 100,000 particles could capture the pattern of solute transport, especially the late-time tailing of BTC, while a smaller number of particles generated more noise in the BTC and a larger number of particles increased the computational burden without significant gain in the quality of the BTCs reconstruction. The mass flux ($\boldsymbol{F}$) across the control plane located at $x = 4{,}000$ m was monitored. Eight simulations were conducted with different velocities by applying different horizontal hydraulic gradients (denoted as J), which are $J = 0.0001$, 0.0003, 0.0005, 0.001, 0.003, 0.005, 0.008, and 0.01.

For the simulations with the steady-state vertical flow only, 100,000 particles were released initially from a horizontal plane of 1,000 m long and 1,000 m wide at $z = 55$ m. The mass flux across the horizontal control plane located at $z = 10$ m was monitored. Nine vertical hydraulic gradients, including 0.003, 0.005, 0.01, 0.03, 0.05, 0.08, 0.1, 0.15, and 0.2, were simulated.

For each steady-state scenario with different horizontal hydraulic gradients, the mass transfer rate coefficient α used for the upscaled MRMT method was calibrated by fitting the BTC to the corresponding curve for the heterogeneous simulation, which is plotted in supporting information Figure S1. The calibrated α is also listed in Table 3a. The plot of the best fit α versus the velocity for each scenario is depicted in Figure 2a, which reveals a power law relationship with R^2 of 0.98. Therefore, equation (7) can be expressed as

$$\alpha_n = \alpha_1 \left(\frac{v_n}{v_1}\right)^k \tag{9}$$

where the best fit coefficient k is 0.41. For the transient flow system, α_1 is the mass transfer rate coefficient calibrated for the flow system with velocity v_1 under the steady-state flow condition. After the flow field changes, the mass transfer rate coefficient is replaced by α_n given the current velocity v_n.

The power law relationship can also be obtained between the Damkohler numbers (D_a) and the velocity (Figure 2b). D_a is a dimensionless parameter describing the magnitude of nonideal transport associated

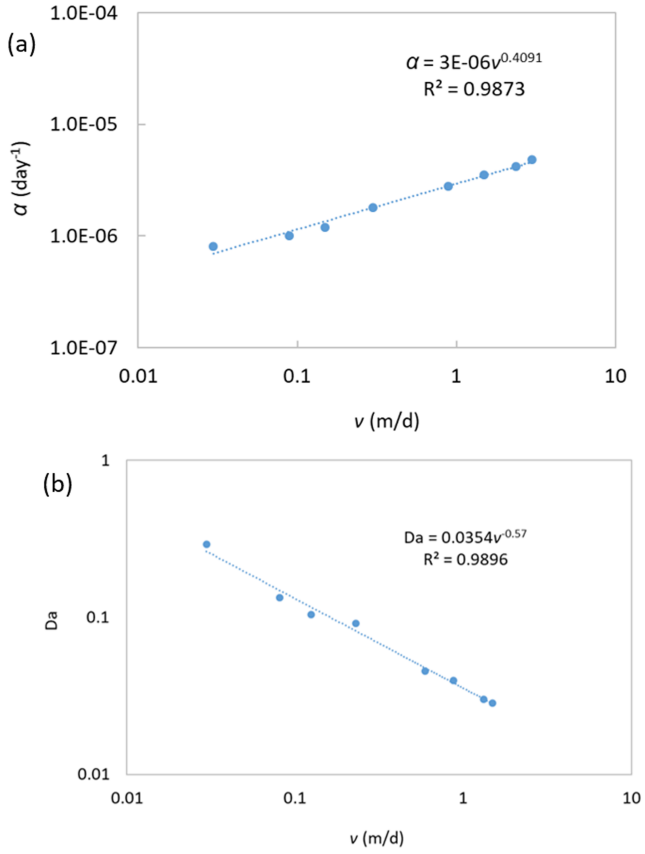

Figure 2. Relationship between velocity and mass transfer rate coefficient for scenarios of solute transport with steady-state horizontal flow (a). Relationship between velocity and D_a (Damkohler number) for scenarios of solute transport with steady-state horizontal flow (b).

with a mass-transfer process and characterizing the ratio of the mass-transfer time scale to the advection time scale, which can be calculated by (Salamon et al., 2006)

$$D_a = [\alpha(\beta + 1)R_m L]/v \tag{10}$$

where L is the domain length (L). According to Figure 2b, the relationship between D_a and v can be written as

$$D_a = Bv^l. \tag{11}$$

Combining equations (10) and (11), we obtain the relationship between β and v:

$$\beta_n = (\beta_1 + 1)\left(\frac{v_n}{v_1}\right)^{l-k+1} - 1 \tag{12}$$

where β_1 is the capacity coefficient calibrated for the steady-state flow system with velocity v_1 and the exponents l and k are defined below.

In this study, the capacity coefficient was determined according to the ratio of the volume of fine materials (clay and silty sand) to the volume of coarse materials (sand and gravel) for the heterogeneous domain, which is fixed for each simulation. Therefore, here we have

$$l = k - 1 \tag{13}$$

resulting in $l = -0.52$, which is close to the value of -0.57 obtained from the relationship between D_a and v plotted in Figure 2b.

For the scenarios with the vertical flow only, α was calibrated the same way as the simulations with the horizontal flow only (Table 3b). The power law relationship was also built between α and v and D_a and v as shown in Figure 3. In Figure 3b, $l = -0.05$, which is different from the horizontal domain. Notably, in this study, we determined β for both horizontal-flow system and vertical-flow system according to its physical meaning proposed in the literature (e.g., Haggerty et al., 2004; Zhang et al., 2014). The capacity coefficient β can also change with the flow velocity according to (13). However, previous studies showed that the total capacity coefficient β can be approximated by the volumetric ratio of the immobile phase and the mobile phase (Haggerty et al., 2000; Zhang et al., 2014). Our tests showed that this hypothesis, which leads to a value of $\beta = 2$ using the hydrofacies model built in this study, can be used to efficiently approximate the measured BTCs for transport under a steady-state flow. Hence, to reduce the number of unknown parameters, we fix the total capacity coefficient β in the following study.

3. Application of aMMT

Solute transport under either the transient horizontal or vertical flow (due to, e.g., time-dependent land or water management) was simulated for heterogeneous and upscaled homogeneous domains using both the MRMT and aMMT methods.

For the simulations with the transient horizontal flow only, two scenarios were considered. In the first scenario, the horizontal hydraulic gradient was 0.01 initially and then dropped to 0.001 at the year of 20, resulting in the declined regional velocity. The second scenario simulated the opposite change of the velocity with the initial hydraulic gradient 0.001 followed by 0.01 when the time t reached 200 years.

For the simulations with the transient vertical flow only, the transient scenarios were simulated by changing the vertical hydraulic gradient from 0.1 to 0.001 (i.e., J decreased with time) or from 0.05 to 0.2 (i.e., J increased with time). Additional scenarios with smaller flow rates were also simulated with the vertical hydraulic gradient decreasing from 0.001 to 0.0001 or increasing from 0.001 to 0.01 at time t = 10,000

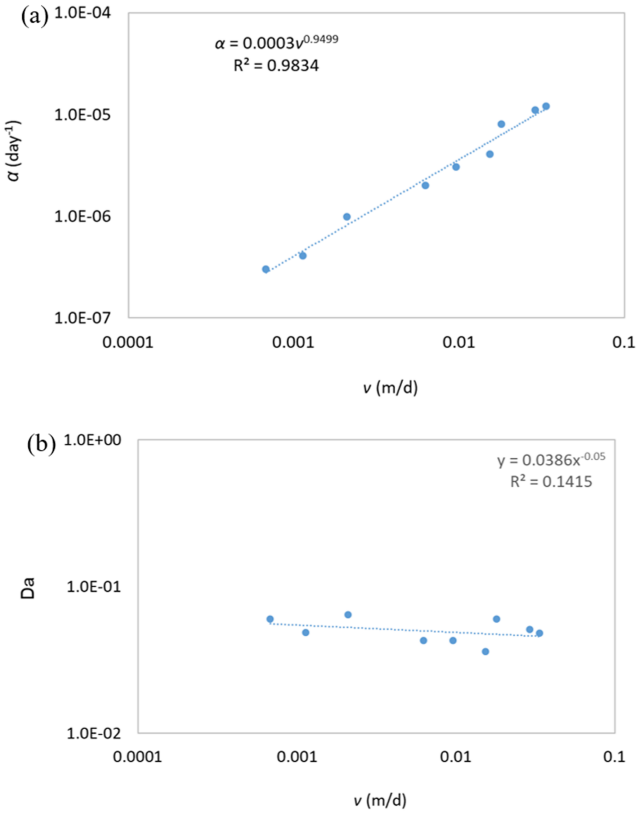

Figure 3. Relationship between velocity and mass transfer rate coefficient for scenarios of solute transport with steady-state vertical flow (a). Relationship between velocity and D_a (Damkohler number) for scenarios of solute transport with steady-state horizontal flow (b).

years. For simulations conducted with vertical flow only, the low K_v values result in smaller vertical flux. Moreover, because of the stratification of hydrofacies in the system, especially for simulations with low gradient, particles need to bypass the low permeable lenses through circuitous pathways, which can result in even longer travel time. Time $t = 10{,}000$ years was selected as apparent tail is observed during this time. To test the impacts of the flow direction on upscaling parameters, a specific scenario was also developed where the flow changed from vertical only to primarily horizontal flow.

BTCs for the two scenarios with the transient horizontal flow only are plotted in Figure 4. For the first scenario, in the first 20 years, the MRMT method describes the transport observed for the heterogeneous simulation well, and the aMMT method shows the same solution since the same coefficients were applied. After the horizontal hydraulic gradient decreased from 0.01 in the first stress period to 0.001 in the second stress period, the mass flux for the heterogeneous simulation dropped two orders of magnitude and so did the results obtained from the MRMT and aMMT models (Figure 4a). Similarly, the BTCs for transport simulations with the hydraulic gradient increasing from 0.001 to 0.01 (Figure 4b) show that both the MRMT and aMMT methods captured the increasing mass flux due to the enhanced flow rate, and the differences in the BTC tails are not significant. Though results from the aMMT model show a slight improvement in capturing the BTC tailing for heterogeneous simulations, transport results from the heterogeneous simulation did not differ significantly from those of the MRMT simulation (especially the overall pattern of the BTCs shown in Figure 4), indicating that the MRMT method is able to upscale transport under transient flow observed for this specific case. For the two simulations conducted for the transient vertical flow only with the vertical hydraulic gradient increasing from 0.05 to 0.2 or decreasing from 0.1 to 0.01, both the MRMT and aMMT models produced changes in the BTC similar to those of the heterogeneous simulation (Figure 5b).

For simulations conducted with slower flow rates where the vertical hydraulic gradient decreased from 0.001 to 0.0001, the mass flux for MRMT shows a larger drop than that for the heterogeneous simulation (Figure 6a). In addition, the slope for the MRMT BTC's late-time tail in the second stress period apparently differs from that for the heterogeneous simulation. Hence, MRMT fails to represent the actual transport process with the transient vertical flow. Contrarily, the decline of mass flux for aMMT (whose parameters change with transient flow) after the flow field changed is much less than that for MRMT. The aMMT's BTC matches better the BTC for the heterogeneous simulation than the MRMT model, especially for the late-time tailing of the BTC. Therefore, in this case, aMMT provides an improved solution to upscale transport with a transient boundary condition. The same result can be found when the vertical hydraulic gradient increased from 0.001 to 0.01 (Figure 6b).

For the last simulation where the flow field changed from vertical flow only to primarily horizontal flow, the performance of MRMT is less satisfying for represent the tail of the BTC observed for the heterogeneous simulation (Figure 7). In addition, the aMMT method could not capture the BTC tails after the boundary condition changed, which is due to the change of the general flow direction (Figure 7). For the aMMT method, although the mass transfer rate coefficients were adjusted according to the flow rates (see section 2.3.3), the abrupt change of the flow direction was not involved in the update of α. Therefore, when the primary flow direction changes, although the aMMT model performs better than the MRMT model, it still deviates noticeably from the heterogeneous case.

The rate coefficient α, which is not a vector but a scalar, was first fitted for steady-state flow along each direction and then used to predict transient flow where the flow direction changed from horizontal to vertical.

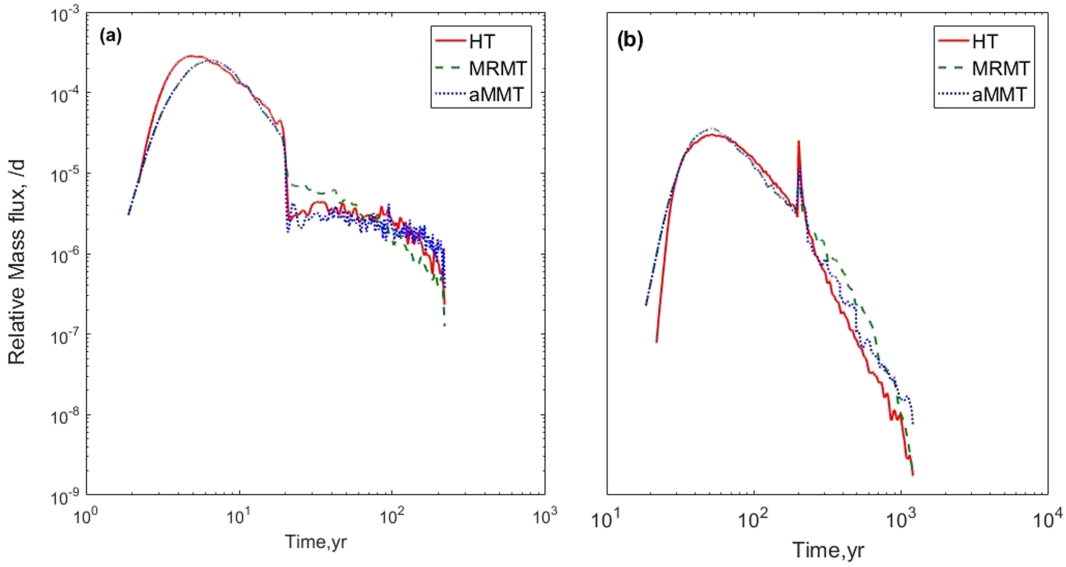

Figure 4. BTCs for transport with the transient horizontal flow only (due to the horizontal hydraulic gradient): The horizontal hydraulic gradient decreased from 0.01 to 0.001 at Year 20 (a); and the horizontal hydraulic gradient increased from 0.001 to 0.01 at Year 200 (b).

When the flow direction changed, the best fit α was quite different (i.e., orders of magnitude different) for the same velocity along different directions. Our tests showed that the parameter α fitted independently along each direction under steady-state flow cannot sufficiently predict transient anomalous transport due to the change of flow directions, implying that transient anomalous transport might be significantly affected by the possible mixing of solutes transported along different directions and/or the initial solute mass partition in the hydrofacies model with complex internal structures, a subtle impact that cannot be efficiently captured by simply combining transport dynamics observed from each direction.

Here we calculated the late-time slopes of the BTCs for the heterogeneous, MRMT, and aMMT models shown in Figures 4–7, the errors between the slopes for the heterogeneous and MRMT models, and the errors between the heterogeneous and aMMT models, using the methods in Guo, Fogg, and Henri (2019), to quantitatively evaluate the model discrepancy. The results are listed in Table 4, which are consistent with the observations from the figures. For example, the errors between the heterogeneous and MRMT models and the ones between the heterogeneous and aMMT models are not significantly different for the tails shown in Figures 4 and 5, whereas in Figure 6, the errors for the aMMT models are much smaller than the ones for the MRMT models. In Figure 7, both models show large errors.

4. Discussion

4.1. Diffusion Versus Slow Advection-Dominated Transport

The simulation results presented above show that MRMT can upscale transport in the transient flow fields with an increasing or decreasing flow rate, but it cannot capture the late-time dynamics of solute transport in transient flow with a very small flow rate or a dramatic change in the main flow direction. Here we calculate the Peclet number (P_e) for these cases to identify the process that dominates solute transport in the heterogeneous systems. *Pe* is determined by

$$Pe = \frac{t_D}{t_A} = \frac{\overline{v_{clay}}}{D^* l} \tag{14}$$

where t_D (T) and t_A (T) are the characteric time for diffusion and advection, $\overline{v_{clay}}$ (LT^{-1}) is the average veloctiy in the clay, D^*($L^2\,T^{-1}$) is the diffusion coefficient, and l (L) is mean length of the clay (Table 2). Results show that for the simulations where MRMT provides a good representation, the corresponding Peclet numbers are larger than 1, representing a slow advection-dominated system. Whereas for the simulations with slower

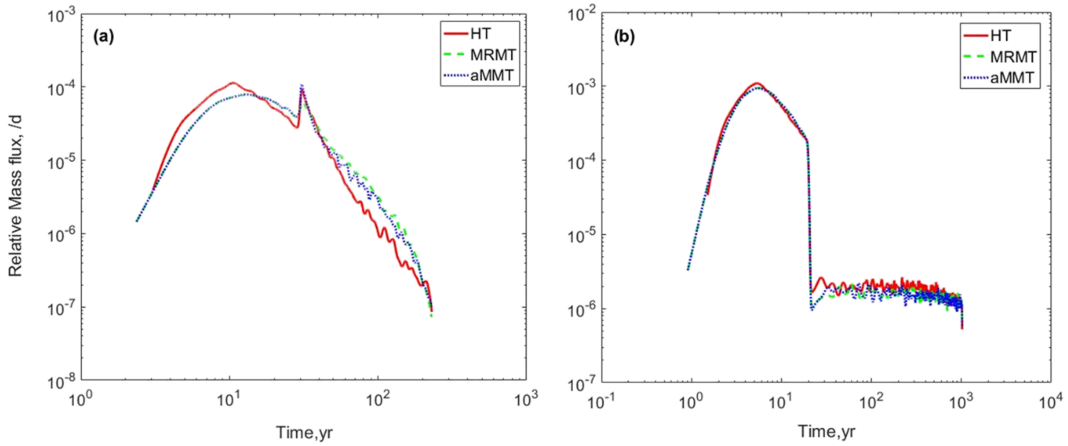

Figure 5. BTCs for the transport simulations with the time-dependent vertical hydraulic gradient only: The vertical hydraulic gradient increased from 0.05 to 0.2 (a); or the vertical hydraulic gradient decreased from 0.1 to 0.01 (b) at Year 20.

flow rates, the Peclet numbers are less than 1, representing a diffusion-dominated system. These results are consistent with those identified by Guswa and Freyberg (2000), who distinguished the slow advection and diffusion processes in low permeability zones and their impacts on transport.

The impact of P_e on transport and its upscaling can be further demonstrated by evaluating the sensitivity of solute dynamics to the diffusion coefficient used in the heterogeneous model simulations. Figure 8 shows BTCs for the heterogeneous model simulations conducted with different diffusion coefficients ($D^* = 10^{-4}$ and 10^{-5} m^2/day) for the horizontal hydraulic gradient of 0.001 whose P_e is greater than 1 (Figure 8a) and the vertical hydraulic gradient of 0.0001 whose P_e is less than 1 (Figure 8b). In Figure 8a, with one order of magnitude difference in the diffusion coefficient, a minimal discrepancy is observed between the two BTCs; whereas for the simulation with $P_e < 1$, the BTC is sensitive to the diffusion coefficient D^*, whose variation results in quite different early arrivals and late-time tails in the BTC (Figure 8b).

Therefore, for the slow advection-dominated system, both MRMT and aMMT can provide a reasonable representation of the transport behavior observed in the heterogeneous simulations, since the solute

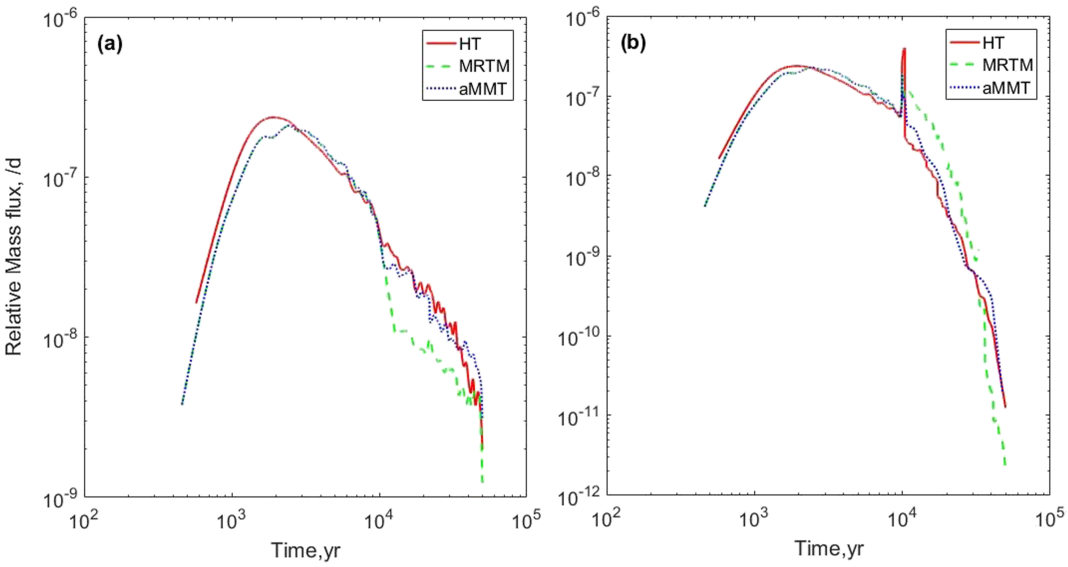

Figure 6. BTCs for solute transport simulations with a small vertical hydraulic gradient. At time t = 10,000 years, the vertical hydraulic gradient decreased from 0.001 to 0.0001 (a) or increased from 0.001 to 0.01 (b).

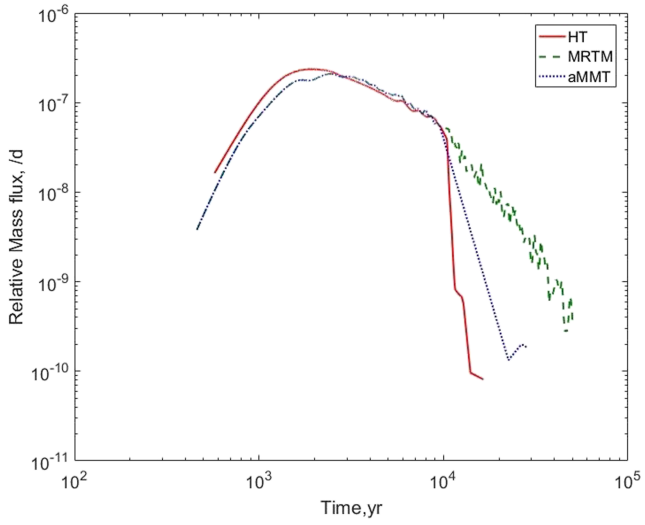

Figure 7. BTCs for solute transport simulations with transient flow, where the general flow direction changed from vertical to primarily horizontal.

particles across the control plane are migrating with the flow field. For these systems, when the boundary condition changes, the flow field will change accordingly and so does the particle transport process. The mass transfer process (via molecular diffusion between mobile and the relatively immobile zones) has less impacts on the main dynamics compared to the advection process therefore, when the boundary condition changes and groundwater flow becomes transient (note here the main flow direction cannot change dramatically, as that shown in Figure 7), MRMT may still capture the anomalous transport behavior affected by subgrid heterogeneity under transient flow conditions.

For the diffusion-dominated system, the transport behavior especially the late-time BTC tail is controlled by the diffusion process, which was assumed to be efficiently captured by the mass transfer term in the MRMT simulations (Haggerty et al., 2000; Haggerty & Gorelick, 1995). The change of the flow field results in the change in diffusion, which then causes the change of transport behaviors in the heterogeneous simulation. Therefore, the mass transfer coefficient matching the previous velocity in MRMT can no longer capture the updated diffusion in transient flow. Contrarily, the aMMT method adjusts the mass transfer coefficients based on the relationship between flow fields and mass transfer coefficients, leading to a better representation of transport under transient flow conditions for diffusion-dominated systems (Figure 6).

4.2. Mass Distribution

Here we calculate the mass distribution for solutes in mobile and immobile zones for MRMT and aMMT systems and the mass distribution in the coarse (gravel and sand) and finer materials (silty sand and clay) for the heterogeneous systems. Results for the simulation with the horizontal-only hydraulic gradient decreasing from 0.01 to 0.001 are plotted in Figure 9, where the mass in clay and silty sand for the heterogeneous scenarios can be compared with the mass in the immobile zones for MRMT and aMMT scenarios. MRMT fails to appropriately represent the mass distribution in coarse and fine materials for the heterogeneous scenarios (Figure 9a), which is consistent with the result in Guo, Fogg, and Henri (2019). In contrast, aMMT provides a better representation of the immobile mass by adjusting the mass transfer rate coefficients. Therefore, appropriately modeling the mass transfer process can improve performance of simulating not only the BTCs but also the mass distribution among aquifer and aquitard facies over time.

It is also noteworthy that most of the solute mass is trapped in the fine deposits in the hydrofacies models (Figure 9), resulting in strong subdiffusive anomalous transport or solute retention, which requires a large capacity coefficient β and/or a small mass exchange rate α in the MRMT or aMMT model (such as those listed in Table 3). Note that the mass shown in Figure 9 is the solute mass remaining in the model domain. Some particles exit the model domain during the modeling period, so the total mass does not remain stable. This explains why the summation of mass for HT is much larger than that for MRMT shown in Figure 9a.

Table 4
Late-Tail Slopes, Errors Between Heterogeneous and MRMT Models, and Errors Between Heterogeneous and aMMT Models

	Slope			Error	
	HT	MRMT	aMMT	MRMT	aMMT
Figure 4a	−1.19	−1.28	−1.14	−7.56%	4.20%
Figure 4b	−4.06	−4.69	−3.28	−15.52%	−9.32%
Figure 5a	−3.33	−3.35	−3.40	−0.60%	2.17%
Figure 5b	−0.04	−0.04	−0.04	4.75%	4.25%
Figure 6a	−1.20	−0.95	−1.18	20.83%	1.67%
Figure 6b	−5.11	−6.63	−5.39	−29.75%	−5.48%
Figure 7	−20.20	−3.02	−7.07	85.05%	−64.99%

4.3. Challenges of Transport Upscaling Using aMMT

The aMMT method presented in this study improves the classical MRMT method in upscaling transport under transient flow conditions for diffusion-dominated systems with a fixed primary flow direction, which indicates that including the velocity into the upscaling process can be helpful when solving transport in transient flow fields. However, when the primary flow direction changes, such as the case presented above where the vertical flow changes to the horizontal flow (e.g., potentially caused by reduction of pumping that previously increased the vertical flow), aMMT fails to capture the tails in the BTCs observed for the heterogeneous systems. Vice versa, with initiation of extensive pumping in a basin, the flow field can be changed dramatically, especially the flow direction. Without involving the flow direction into consideration,

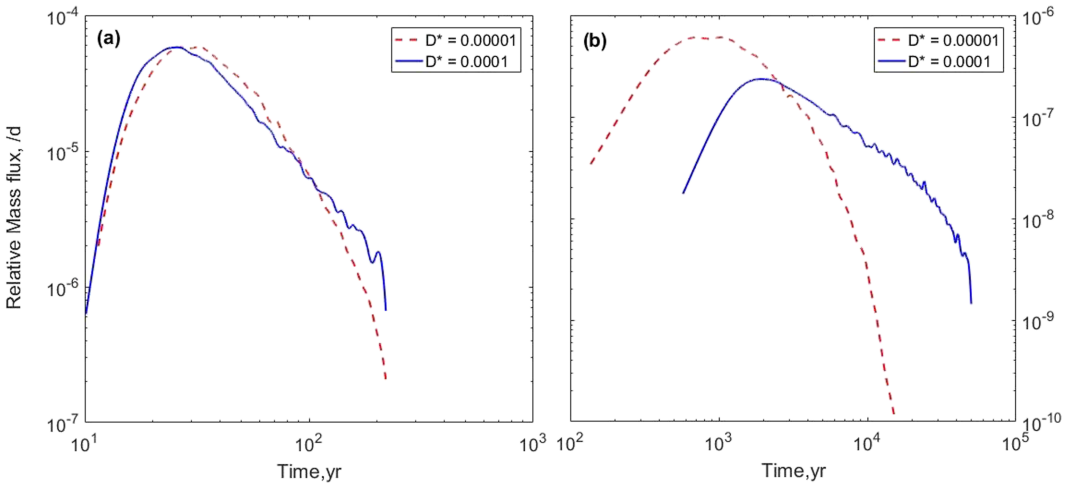

Figure 8. BTCs for transport in steady-state flow fields with a small vertical hydraulic gradient and different diffusion coefficients D^*. In (a), the horizontal hydraulic gradient is 0.001, and P_e is greater than 1 (i.e., advection-dominated transport). In (b), the vertical hydraulic gradient is 0.0001, and P_e is less than 1 (i.e., diffusion-dominated transport).

aMMT cannot represent the transport under these transient conditions. Therefore, even though the model fitting can be improved by adjusting the mass transfer rate coefficient with the flow rate, the next question of how to adapt the mass transfer rate coefficient with a changing flow direction remains a challenge. This issue is important for systems in which changes in pumping, recharge, or both induce significant transients in rates and direction of flow.

One possible solution for the aMMT model fitting with a time-variable flow direction may be the incorporation of the medium's internal structure into the estimation of mass transfer parameters. Non-Fickian transport in heterogeneous media including alluvial settings was found to be affected by the architecture of the

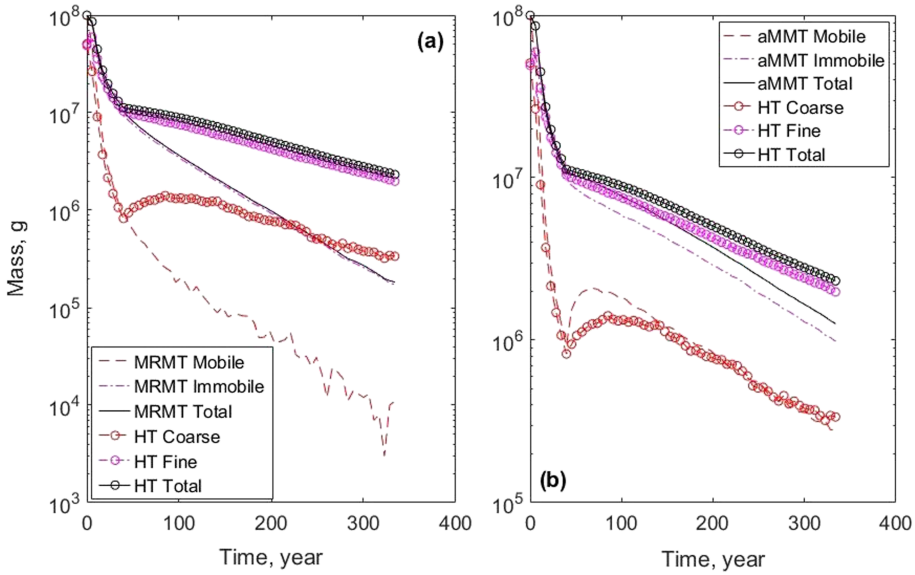

Figure 9. Evolution of solute mass in each phase for the upscaling models (lines) and the heterogeneous simulations (symbols on line) under transient boundary conditions with the horizontal hydraulic gradient decreasing from 0.01 to 0.001 at time $t = 20$ years. Mobile mass for the MRMT and aMMT models was compared with the mass in the coarse materials for the heterogeneous simulation; and the immobile mass for MRMT and aMMT was compared with the mass in the fine materials for the heterogeneous simulation. (a) Mass distribution for MRMT and heterogeneous simulations and (b) mass distribution for aMMT and heterogeneous simulations.

medium, such as the probability density function (PDF) of thickness of relatively low-permeability layers which controls the random residence time for solute particles and therefore dominates the late-time tailing behavior of tracer BTCs (Zhang et al., 2014). The medium internal structure can affect the effective flow velocity, while the effective flow velocity cannot represent the overall medium heterogeneity to define the nonlocal transport parameters (especially the mass transfer rate) controlling the whole process of solute retention. On one hand, when the flow direction is fixed in the transient flow, the PDF of the thickness of the low-permeability deposits is also fixed. The corresponding solute transport behavior, such as subdiffusion, which is mainly driven by the solute retention process and is defined as transport where the plume variance grows slower than linear in time, is affected by and then can be statistically correlated with the overall flow velocity. A similar conclusion was found by Levy and Berkowitz (2003) using laboratory column transport experiments, where the subdiffusive transport dynamics changed with the general hydraulic gradient across the sand column. On the other hand, the change of the flow direction alters the PDF of the thickness of the low-permeability deposits encountered by a solute resulting in a different relationship between the mass transfer rate coefficient and the effective flow velocity. For example, when the flow direction changes from the horizontal to the vertical direction, solutes must move through more aquitard layers because the horizontal mean length for lithofacies is much larger than the vertical mean length, leading to stronger subdiffusion with a heavier late-time tail in the BTC. This characteristic is evident when comparing the two scenarios shown in Figures 4 and 5: The late-time tail of the resultant BTC is much heavier for groundwater flow along the vertical direction (Figure 5) than the horizontal direction (Figure 4). The opposite case is shown in Figure 7, where the BTC's late-time tail drops much faster (i.e., a lighter tail) after the general flow direction changes from the vertical to the horizontal direction, due to the apparent decrease of both the effective thickness of low-permeability lithofacies encountered by the flow field and the random residence times of solute particles. We will improve the aMMT method by incorporating the medium's heterogeneity into the estimation of α and β in a future study, by, for example, extending the work of Zhang et al. (2014).

Application of the aMMT method developed in this study requires the relationship between coefficients and flow rates, which is determined by conducting the heterogeneous simulations under steady-state flows. This relationship can be also generated by conducting tracer tests in the field or lab experiments with different velocities. The method provides a promising direction solving the transient transport in complex systems.

Although it might be prudent to conduct these experiments on more than one heterogeneous realization, we point out that transport in multifacies systems like this tends to be dominated by the connectivity of the high-K facies (see also LaBolle & Fogg, 2001; Fogg et al., 2000). This is also the reason that the capacity coefficient β in the aMMT method can be approximated by the ratio of global volumetric proportions of the fine and coarse hydrofacies. In addition, the hydrofacies models contain abundant hard conditional data obtained from hundreds of boreholes, which can decrease the variation between realizations, and hence, one hydrofacies model may capture the overall flow/transport behavior similar to the other models. Nevertheless, further tests using additional realizations and various source sizes should be conducted in future studies.

4.4. Parameters in aMMT and Other Time-Nonlocal Transport Models

The core parameters in the aMMT model that capture anomalous transport are the pairs of the rate coefficient α_i and the capacity coefficient β_i. The rate coefficient α_i describes the (inverse of the) diffusive time for solute particles to exit the ith immobile domain, which is simplified as the spherical low-permeability block in this study (see Table 1), while the capacity coefficient β_i describes the (normalized) volumetric proportion of the ith immobile domain (see Zhang, Benson, Meerschaert, & LaBolle, 2007, for further discussion of the physical meanings of each MRMT parameter). Fitting exercises in this study show that the rate coefficient α increases with an increasing effective velocity v (Figures 2a and 3a), which is expected because the dispersion coefficient is well-known to increase with velocity. It is also noteworthy that the power law relationship between α_i and v is sensitive to the flow direction. Particularly, the rate coefficient α_i increases almost as the square root of v (although quantitative explanation is needed for this square root relationship in a future study) for flow along the longitudinal direction, while α_i increases almost linearly with v for flow along the vertical direction. This discrepancy implies that plume dispersion for the well-connected porous medium with channeling flow is relatively less sensitive to the overall hydraulic gradient than that in the medium with more discrete lithofacies.

The MRMT model in this study used finite spherical blocks to approximate the irregular immobile domains, whose impact on solute transport may also be approximated by the CTRW framework (Berkowitz et al., 2006), the tempered temporal fADE (Zhang et al., 2015), and the phase exposure-dependent exchange model (Ginn et al., 2017) using a truncated power law (TPL) memory function. Particularly, the late-time BTC slope exhibits a TPL (with the well-known 3/2 slope for matrix diffusion) for the standard finite spherical model (Haggerty et al., 2000), and this implies that the TPL memory function in the CTRW framework and the tempered temporal fADE has an exponent of $-3/2$ and a truncation parameter on the order of the smallest rate coefficient in the MRMT model. The corresponding remobilization rate coefficient in the phase exposure-dependent exchange model can also be derived using the TPL memory function, according to equation (2) in Ginn et al. (2017). For transient flow, however, the applicability of these time nonlocal transport models remains to be shown. For example, the standard CTRW framework was developed using the generalized Master equation, which describes a spatial average with stationary jump size and waiting time PDFs for solute particles (without distinguishing the mobile and immobile status) (Berkowitz et al., 2006). New derivations are needed for a transient memory function. The standard temporal fADE models are the scaling limit of random walking particles with infinite mean waiting times, and hence, improvement including the variable index is needed to update the fADE to capture anomalous transport under the transient flow condition.

5. Summary and Conclusions

This study explored the upscaling of anomalous transport under transient flow conditions by combining the mass transfer models and numerical simulations of flow and transport in regional-scale aquifers. The aMMT method was developed and tested under different transient boundary conditions. The method was modified from the conventional MRMT model by updating the mass transfer rate coefficient with the flow fields in every stress period instead of using a fixed mass transfer rate coefficient through the whole transport period. Advective-dispersive contaminant transport was first simulated in a 3-D heterogeneous domain and used as a reference solution for model upscaling. Equivalent transport under homogeneous flow conditions were then evaluated by applying the MRMT model and aMMT model. The mass transfer coefficients were determined by fitting the BTCs for the MRMT model to the corresponding BTCs for the heterogeneous simulations under the steady-state flow for scenarios including horizontal flow (parallel to strata) and vertical flow (perpendicular to strata). This study provided insights on upscaling transport under transient flow conditions, which is needed to accommodate the needs for regional-scale groundwater management and remediation in which transient changes in pumping and recharge and their subsequent effects on directions and rates of groundwater flow occur. Four main conclusions were drawn from this study.

First, a power law relationship was obtained between the mass transfer rate coefficient and the equivalent flow velocity by conducting groundwater flow and solute transport simulations with different hydraulic gradients, which was then used to update the mass transfer rate coefficients at each stress period under transient flow conditions in the aMMT method. This resulted in improved performance in the cases where primary flow direction does not change and transport is dominated by diffusion but not in cases where migration of particles is dominated by advection or in those flow direction is changed.

Second, the Peclet number affects performance of the upscaling method. For example, results indicated that for the slow advection-dominated systems, both MRMT and aMMT can represent transport observed for heterogeneous systems under transient flow conditions. Because the migration of solute particles is dominated by advection, the mass transfer impacts are less significant for solute transport. Whereas for the diffusion-dominated systems, MRMT fails to capture the tails after the boundary condition changes, but the results from aMMT are much more improved. As for these systems, mass transfer due to molecular diffusion plays an important role in solute migration, and therefore, treating the mass transfer rate coefficients as functions of velocity improves results as compared to the traditional MRMT method.

Third, the aMMT model generates more accurate mass distribution in mobile and immobile zones (than the MRMT model) that are closer to the amount of mass residing in coarse and fine materials in the heterogeneous systems. Transient flow may reorganize the flow and stagnant zones and therefore repartition mobile and immobile masses, a process that can be efficiently captured by the velocity-dependent capacity coefficient used in the aMMT model. The dramatic change of mass partitioning in mobile and immobile zones

observed for transient flow causes the abrupt change of anomalous transport dynamics, including the change of the BTC's late-time tailing, which cannot be captured by the standard mass transfer or probably the time nonlocal transport models with fixed rate coefficients.

Fourth, if the flow direction changes dramatically, both MRMT and aMMT fail to capture the tail of the BTCs generated by the heterogeneous systems. Therefore, the next challenge is to quantify the impact of flow direction on the mass transfer process, by, for example, incorporating the medium's internal structure, such as the thicknesses of low-permeability deposits or the relatively immobile zones encountered by groundwater flow fields, into the estimation of the rate and capacity coefficients in the aMMT model.

Acknowledgments
This research was supported by the U.S. Department of Energy, Cerc-Wet program; the National Natural Science Foundation of China (41931292); Guangdong Provincial Key Laboratory of Soil and Groundwater Pollution Control (2017B030301012); and State Environmental Protection Key Laboratory of Integrated Surface Water-Groundwater Pollution Control. Data used in this work are available at the website (https://doi.org/10.15146/R3NM3S).

References

Anastasiadis, P. (2004). Evaluating non-point source pollution using GIS. *Fresenius Environmental Bulletin*, *13*(11A), 1168–1172.

Baeumer, B., Zhang, Y., & Schumer, R. (2015). Incorporating super-diffusion due to sub-grid heterogeneity to capture non-Fickian transport. *Ground Water*, *53*(5), 699–708. https://doi.org/10.1111/gwat.12267

Benson, D. A., Schumer, R., Meerschaert, M. M., & Wheatcraft, S. W. (2001). Fractional dispersion, Lévy motion, and the MADE tracer tests. *Transport in Porous Media*, *42*, 211–240.

Benson, D. A., Wheatcraft, S. W., & Meerschaert, M. M. (2000a). The fractional-order governing equation of Lévy motion. *Water Resources Research*, *36*(6), 1413–1423.

Benson, D. A., Wheatcraft, S. W., & Meerschaert, M. M. (2000b). Application of a fractional advection–dispersion equation. *Water Resources Research*, *36*(6), 1403–1412.

Berkowitz, B., Cortis, A., Dentz, M., & Scher, H. (2006). Modeling non-Fickian transport in geological formations as a continuous time random walk. *Reviews of Geophysics*, *44*, RG2003. https://doi.org/10.1029/2005RG000178

Berkowitz, B., & Scher, H. (1995). On characterization of anomalous dispersion in porous and fractured media. *Water Resources Research*, *31*, 1461–1466.

Berkowitz, B., & Scher, H. (1998). Theory of anomalous chemical transport in random fracture networks. *Physical Review E*, *57*, 5858–5869.

Bianchi, M., Zheng, C., Wilson, C., Tick, G. R., Liu, G., & Gorelick, S. M. (2011). Spatial connectivity in a highly heterogeneous aquifer: From cores to preferential flow paths. *Water Resources Research*, *47*, W05524. https://doi.org/10.1029/2009WR008966

Bolster, D., Benson, D. A., Le Borgne, T., & Dentz, M. (2010). Anomalous mixing and reaction induced by superdiffusive nonlocal transport. *Physical Review E*, *82*(2), 021119.

Brusseau, M. L., & Guo, Z. (2014). Assessing contaminant-removal conditions and plume persistence through analysis of data from long-term pump-and-treat operations. *Journal of Contaminant Hydrology*, *164*, 16–24. https://doi.org/10.1016/j.jconhyd.2014.05.004

Brusseau, M. L., Hatton, J., & DiGuiseppi, W. (2011). Assessing the impact of source-zone remediation efforts at the contaminant-plume scale through analysis of contaminant mass discharge. *Journal of Contaminant Hydrology*, *126*(3-4), 130–139. https://doi.org/10.1016/j.jconhyd.2011.08.003

Brusseau, M. L., Nelson, N. T., Zhang, Z., Blue, J. E., Rohrer, J., & Allen, T. (2007). Source-zone characterization of a chlorinated-solvent contaminated superfund site in Tucson, AZ. *Journal of Contaminant Hydrology*, *90*, 21–40.

Carle, S. F. (1997). Implementation schemes for avoiding artifact discontinuities in simulated annealing. *Mathematical Geology*, *29*(20), 231–244.

Carle, S. F., & Fogg, G. E. (1996). Transition probability-based indicator geostatistics. *Mathematical Geology*, *28*(4), 453–477.

Carle, S. F., & Fogg, G. E. (1997). Modeling spatial variability with one- and multi-dimensional continuous Markov chains. *Mathematical Geology*, *29*(7), 891–917.

Carle, S. F., LaBolle, E. M., Weissmann, G. S., Van Brocklin, D., & Fogg, G. E. (1998). Conditional simulation of hydrofacies architecture: Atransition probability/Markov chain approach. In G. S. Fraser & J. M. Davis (Eds.), *Hydrogeologic Models of Sedimentary Aquifers*, Concepts Hydrogeol. Environ. Geol. Ser. (Vol. 1, pp. 147–170). Tulsa, OK: Society for Sedimentary Geology

Carrera, J., & Neuman, S. P. (1986). Estimation of aquifer parameters under transient and steady-state conditions. 1. Maximum likelihood method incorporating prior information. *Water Resources Research*, *22*(2), 199–210.

Carrera, J., Sanchez-Vila, X., Benet, I., Medina, A., Galarza, G., & Guimera, J. (1998). On matrix diffusion: Formulations, solution methods and qualitative effects. *Hydrogeology Journal*, *6*, 178–190.

Chae, G. T., Kim, K. J., Yun, S. T., Kim, K. H., Kim, S. O., Choi, B. Y., et al. (2004). Hydrogeochemistry of alluvial ground-waters in an agricultural area: An implication for groundwater contamination susceptibility. *Chemosphere*, *55*(3), 369–378.

Cortis, A., & Berkowitz, B. (2005). Computing "anomalous" contaminant transport in porous media: The CTRW Matlab toolbox. *Ground Water*, *43*(6), 947–950.

Dearden, R. A., Marchant, A., & Royse, K. (2013). Development of a suitability map for infiltration sustainable drainage systems (SuDS). *Environment and Earth Science*, *70*(6), 2587–2602.

Dentz, M., & Berkowitz, B. (2003). Transport behavior of a passive solute in continuous time random walks and multirate mass transfer. *Water Resources Research*, *39*(5), 1111. https://doi.org/10.1029/2001WR001163

Dentz, M., Cortis, A., Scher, H., & Berkowitz, B. (2004). Time behavior of solute transport in heterogeneous media: Transition from anomalous to normal transport. *Advances in Water Resources*, *27*, 155–173.

Edirisinghe, E. A., Karunarathne, G. R., Samarakoon, A. S., Pitawala, H. M., Dharmagunawardhane, H. A., & Tilakarathna, I. A. (2016). Assessing causes of quality deterioration of groundwater in Puttalam, Sri Lanka, using isotope and hydrochemical tools. *Isotopes in Environmental and Health Studies*, *52*(4-5), 513–528. https://doi.org/10.1080/10256016.2015.1127918

Feehley, C. E., Zheng, C., & Molz, F. J. (2000). A dual-domain mass transfer approach for modeling solute transport in heterogeneous porous media, application to the MADE site. *Water Resources Research*, *36*(9), 2501–2515.

Fernàndez-Garcia, D., Illangasekare, T. H., & Rajaram, H. (2005). Differences in the scale dependence of dispersivity estimated from temporal and spatial moments in chemically and physically heterogeneous porous media. *Advances in Water Resources*, *28*(7), 745–759.

Fogg, C. E., Carle, S. F., & Green, C. (2000). Connected-network paradigm for the alluvial aquifer system. In D. Zhang & C. L. Winter (Eds.), *Theory, modeling, and field investigation in hydrogeology: A special volume in Honor of Shlomo P. Neuman's 60th Birthday*, *Special Paper* (Vol. 348, pp. 25–42). Boulder, CO: Geologic. Soc. Am.

Fogg, G. E., & LaBolle, E. M. (2006). Motivation of synthesis, with an example on groundwater quality sustainability. *Water Resources Research*, *42*, W03S05. https://doi.org/10.1029/2005WR004372

Fogg, G. E., LaBolle, E. M., & Weissmann, G. S. (1999). Groundwater vulnerability assessment: Hydrogeologic perspective and example from Salinas Valley, California. In D. L. Corwin, K. Loague, & T. R. Ellsworth (Eds.), *Assessment of Non-point Source Pollution in the Vadose Zone*, *Geophys. Monogr. Ser.* (Vol. 108, pp. 45–61). Washington, DC: American Geophysical Union.

Fogg, G. E., & Zhang, Y. (2016). Debates—Stochastic subsurface hydrology from theory to practice: A geologic perspective. *Water Resources Research*, *52*, 9235–9245. https://doi.org/10.1002/2016WR019699

Ginn, T. R., Schreyer, L. G., & Zamani, K. (2017). Phase exposure-dependent exchange. *Water Resources Research*, *53*, 619–632. https://doi.org/10.1002/2016WR019755

Gorelick, S. M., Liu, G., & Zheng, C. (2005). Quantifying mass transfer in permeable media containing conductive dendritic networks. *Geophysical Research Letters*, *32*, L18402. https://doi.org/10.1029/2005GL023512

Guo, Z., & Brusseau, M. L. (2017). The impact of well-field configuration and permeability heterogeneity on contaminant mass removal and plume persistence. *Journal of Hazardous Materials*, *333*, 109–115. https://doi.org/10.1016/j.jhazmat.2017.03.012

Guo, Z., Fogg, G. E., Brusseau, M. L., Jose, L., & LaBolle, E. M. (2019). Modeling groundwater contaminant transport in the presence of large heterogeneity: A case study comparing MT3D and RWhet. *Hydrogeology Journal*, *27*(4), 1363–1371.

Guo, Z., Fogg, G. E., & Henri, C. (2019). Upscaling of regional scale transport under transient conditions: Evaluation of the multirate mass transfer model. *Water Resources Research*, *55*, 5301–5320. https://doi.org/10.1029/2019WR024953

Guswa, A. J., & Freyberg, D. L. (2000). Slow advection and diffusion through low permeability inclusions. *Journal of Contaminant Hydrology*, *46*(3–4), 205–232.

Haggerty, R., & Gorelick, S. M. (1995). Multiple-rate mass transfer for modeling diffusion and surface reactions in media with pore-scale heterogeneity. *Water Resources Research*, *31*(10), 2383–2400.

Haggerty, R., Harvey, C. F., Freiherr von Schwerin, C., & Meigs, L. C. (2004). What controls the apparent timescale of solute mass transfer in aquifers and soils? A comparison of experimental results. *Water Resources Research*, *40*, W01510. https://doi.org/10.1029/2002WR001716

Haggerty, R., McKenna, S. A., & Meigs, L. C. (2000). On the late-time behavior of tracer test breakthrough curves. *Water Resources Research*, *36*(12), 3467–3479. https://doi.org/10.1029/2000WR900214

Harbaugh, A. W., Banta, E. R., Hill, M. C., & McDonald, M. G. (2000). MODFLOW-2000, The U.S. Geological Survey modular ground-water model-user guide to modularization concepts and the ground-water flow process, U.S. Geological Survey Open-File Report 00-92, 2000.

Harvey, C., & Gorelick, S. M. (2000). Rate-limited mass transfer or macrodispersion: Which dominates plume evolution at the Macrodispersion Experiment (MADE) site? *Water Resources Research*, *36*(3), 637–650.

Henri, C. V., & Fernàndez-Garcia, D. (2014). Toward efficiency in heterogeneous multispecies reactive transport modeling: A particle-tracking solution for first-order network reactions. *Water Resources Research*, *50*, 7206–7230. https://doi.org/10.1002/2013WR014956

Henri, C. V., & Fernàndez-Garcia, D. (2015). A random walk solution for modeling solute transport with network reactions and multi-rate mass transfer in heterogeneous systems: Impact of biofilms. *Advances in Water Resources*, *86*, 199–132.

LaBolle, E. M., & Fogg, G. E. (2001). Role of molecular diffusion in contaminant migration and recovery in an alluvial aquifer system. *Transport in Porous Media*, *42*, 155–179.

Levy, M., & Berkowitz, B. (2003). Measurement and analysis of non-Fickian dispersion in heterogeneous porous media. *Journal of Contaminant Hydrology*, *64*(3-4), 203–226. https://doi.org/10.1016/S0169-7722(02)00204-8

Li, W., Wang, M. Y., Liu, L., & Yan, Y. (2015). Assessment of long-term evolution of groundwater hydrochemical characteristics using multiple approaches: A case study in Cangzhou, Northern China. *Water*, *7*, 1109–1128. https://doi.org/10.3390/w7031109

Liu, G., Zheng, C., & Gorelick, S. M. (2004). Limits of applicability of the advection-dispersion model in aquifers containing connected high-conductivity channels. *Water Resources Research*, *40*, W08308. https://doi.org/10.1029/2003WR002735

Lu, B. Q., Zhang, Y., Zheng, C. M., Green, C. T., O'Neill, C., Sun, H. G., & Qian, J. Z. (2018). Comparison of time nonlocal transport models for characterizing non-Fickian transport: From mathematical interpretation to laboratory application. *Water*, *10*, 778. https://doi.org/10.3390/w10060778

Matthieu, D. E. III, Brusseau, M. L., Guo, Z., Plaschke, M., Carroll, K. C., & Brinker, F. (2014). Persistence of a groundwater contaminant plume after hydraulic source containment at a chlorinated-solvent contaminated site. *Groundwater Monitoring & Remediation*, *34*, 23–32.

McDonald, M. G., & Harbaugh, A. W. (1988). A modular three-dimensional finite-difference ground-water flow model, U.S. Geological Survey Techniques of Water-Resources Investigations. Chapter A1, 586 p.

Nagy, E. (2009). Basic equations of mass transfer through biocatalytic membrane layer. *Asia-Pacific Journal of Chemical Engineering*, *4*, 270–278.

Nativ, R. (2004). Can the desert bloom? Lessons learned from the Israeli case. *Ground Water*, *42*(5), 651–657.

Nissan, A., Dror, I., & Berkowitz, B. (2017). Time-dependent velocity-field controls on anomalous chemical transport in porous media. *Water Resources Research*, *53*, 3760–3769. https://doi.org/10.1002/2016WR020143

Nolan, B. T., Hitt, K. J., & Ruddy, B. C. (2002). Probability of nitrate contamination of recently recharged groundwaters in the conterminous United States. *Environmental Science & Technology*, *26*(10), 2138–2145.

Pedretti, D., & Fernandez-Garcia, D. (2013). An automatic locally-adaptive method to estimate heavily-tailed breakthrough curves from particle distributions. *Advances in Water Resources*, *59*, 52–65.

Pedretti, D., Fernandez-Garcia, D., Sanchez-Vila, X., Bolster, D., & Benson, D. A. (2014). Apparent directional mass-transfer capacity coefficients in three-dimensional anisotropic heterogeneous aquifers under radial convergent transport. *Water Resources Research*, *50*, 1205–1224. https://doi.org/10.1002/2013WR014578

Salamon, P., Fernàndez-Garcia, D., & Gómez-Hernández, J. J. (2006). Modeling mass transfer processes using random walk particle tracking. *Water Resources Research*, *42*, W11417. https://doi.org/10.1029/2006WR004927

Seyedabbasi, M. A., Newell, J. C., Adamson, D. T., & Sale, T. C. (2012). Relative contribution of DNAPL dissolution and matrix diffusion to the long-term persistence of chlorinated solvent source zones. *Journal of Contaminant Hydrology*, *134*, 69–81.

Silva, O., Carrera, J., Kumar, S., Dentz, M., Alcolea, A., & Willmann, M. (2009). A general real-time formulation for multi-rate mass transfer problems. *Hydrology and Earth System Sciences*, *6*(2), 2415–2449.

Sinha, S. P., & Elango, L. (2019). Deterioration of groundwater quality: Implications and management. In A. Singh, D. Saha, & A. Tyagi (Eds.), *Water governance: Challenges and prospects* (pp. 87–101). Singapore: Springer Water. Springer.

Sivasankar, V., Ramachandramoorthy, T., & Chandramohan, A. (2013). Deterioration of coastal groundwater quality in Island and mainland regions of Ramanathapuram District, Southern India. *Environmental Monitoring and Assessment*, *185*(1), 931–944. https://doi.org/10.1007/s10661-012-2604-2

Sokolov, I. M., & Klafter, J. (2006). Field-induced dispersion in subdiffusion. *Physical Review Letters*, *97*(14), 140602. https://doi.org/10.1103/PhysRevLett.97.140602

Tompson, A. F. B., Carle, S. F., Rosenberg, N. D., & Maxwell, R. M. (1999). Analysis of groundwater migration from artificial recharge in a large urban aquifer: A simulation perspective. *Water Resources Research*, *35*(10), 2981–2998.

Vengosh, A., Gill, J., Davisson, M. L., & Hudson, G. B. (2002). A multi-isotope (B, Sr, O, H, and C) and age dating (^{3}H–^{3}He and ^{14}C) study of groundwater from Salinas Valley, California: Hydrochemistry, dynamics, and contamination processes. *Water Resources Research*, *38*(1), 1008. https://doi.org/10.1029/2001WR000517

Weissmann, G. S., Zhang, Y., LaBolle, E. M., & Fogg, G. E. (2002). Dispersion of groundwater age in an alluvial aquifer system. *Water Resources Research*, *38*(10), 1198. https://doi.org/10.1029/2001WR000907

Willmann, M., Carrera, J., & Sánchez-Vila, X. (2008). Transport upscaling in heterogeneous aquifers: What physical parameters control memory functions? *Water Resources Research*, *44*, W12437. https://doi.org/10.1029/2007WR006531

Zektser, I. S., & Everett, L. G. (Eds.) (2004). Groundwater resources of the world and their use, Ser. Groundwater, vol. 6, 342 pp., Int. Hydrol. Programme, U. N. Educ., Sci., and Cultural Organ., Paris.

Zhang, H., Harter, T., & Sivakumar, B. (2006). Nonpoint source solute transport normal to aquifer bedding in heterogeneous, Markov chain random fields. *Water Resources Research*, *42*, W06403. https://doi.org/10.1029/2004WR003808

Zhang, Y., Benson, D. A., & Baeumer, B. (2007). Predicting the tails of breakthrough curves in regional-scale alluvial systems. *Ground Water*, *45*(4), 473–484. https://doi.org/10.1111/j.1745-6584.2007.00320.x

Zhang, Y., Benson, D. A., Meerschaert, M. M., & LaBolle, E. M. (2007). Space-fractional advection–dispersion equations with variable parameters: Diverse formulas, numerical solutions, and application to the macrodispersion experiment site data. *Water Resources Research*, *43*, W05439. https://doi.org/10.1029/2006WR004912

Zhang, Y., Green, C., & Baeumer, B. (2014). Linking aquifer spatial properties and non-Fickian transport in mobile-immobile like alluvial settings. *Journal of Hydrology*, *512*, 315–331.

Zhang, Y., LaBolle, E. M., & Pohlmann, K. (2009). Monte Carlo approximation of anomalous diffusion in macroscopic heterogeneous media. *Water Resources Research*, *45*, W10417. https://doi.org/10.1029/2008WR007448

Zhang, Y., Meerschaert, M. M., Baeumer, B., & LaBolle, E. M. (2015). Modeling mixed retention and early arrivals in multidimensional heterogeneous media using an explicit Lagrangian scheme. *Water Resources Research*, *51*, 6311–6337. https://doi.org/10.1002/2015WR016902

Zhang, Z., & Brusseau, M. L. (1998). Characterizing three-dimensional hydraulic conductivity distributions using qualitative and quantitative geologic borehole data: Application to a field site. *Ground Water*, *36*, 671–678.

Zhang, Z., & Brusseau, M. L. (1999). Nonideal transport of reactive solutes in heterogeneous porous media 5. Simulating regional-scale behavior of a trichloroethene plume during pump-and-treat remediation. *Water Resources Research*, *35*, 2921–2935.

Zheng, C., Bianchi, M., & Gorelick, S. M. (2010). Lessons learned from 25 years of research at the MADE site. *Ground Water*, *49*(5), 649–662. https://doi.org/10.1111/j.1745-6584.2010.00753.x

Zheng, C., & Gorelick, S. M. (2003). Analysis of solute transport in flow fields influenced by preferential flow paths at the decimeter scale. *Ground Water*, *41*(2), 142–155. https://doi.org/10.1111/j.1745-6584.2003.tb02578.x

Zheng, C., & Wang, P. P. (1999). MT3DMS: A modular three-dimensional multispecies model for simulation of advection, dispersion and chemical reactions of contaminants in groundwater systems; documentation and user's guide. Contract Report SERDP-99-1, US Army Engineer Research and Development Center, Vicksburg, MS.

Zinn, B., & Harvey, C. F. (2003). When good statistical models of aquifer heterogeneity go bad: A comparison of flow, dispersion, and mass transfer in connected and multivariate Gaussian hydraulic conductivity fields. *Water Resources Research*, *39*(3), 1051. https://doi.org/10.1029/2001WR001146